Numerical Simulation of Orbiting Black Holes

Bernd Brügmann, Wolfgang Tichy, and Nina Jansen
Center for Gravitational Physics and Geometry and Center for Gravitational Wave Physics, Penn State University, University Park, Pennsylvania 16802, USA
(Received 26 December 2003; published 24 May 2004)

We present numerical simulations of binary black hole systems which for the first time last for about one orbital period for close but still separate black holes as indicated by the absence of a common apparent horizon. An important part of the method is the construction of comoving coordinates, in which both the angular and the radial motion are minimized through a dynamically adjusted shift condition. We use fixed mesh refinement for computational efficiency.

DOI: 10.1103/PhysRevLett.92.211101 PACS numbers: 04.25.Dm, 04.30.Db, 95.30.Sf

One of the fundamental problems of general relativity is the two body problem of black holes in a binary orbit. Since in general relativity two orbiting bodies emit gravitational waves that carry away energy and momentum from the system, the two black holes spiral inward and eventually merge. Gravitational waves from black hole mergers are expected to be among the primary sources for gravitational wave astronomy [1,2].

The last few orbits of a black hole binary fall into the strongly dynamic and nonlinear regime of general relativity, and we therefore turn to numerical simulations to solve the full Einstein equations. Numerical relativity has seen many advances in recent years, but so far it has not been possible to simulate even a single binary black hole orbit. The first 3D simulation of a Schwarzschild black hole was performed in 1995 [3]. In [4], the first 3D simulation of spinning and moving black holes in a "grazing collision" of nearby black holes inside an innermost stable circular orbit (ISCO) was presented; see also [5,6]. Simulations starting near or even somewhat outside an ISCO have been performed, e.g., in [7–10], but after rather short evolution times numerical simulations of black hole binaries become unstable. In typical advanced simulations the evolution time before merger is less than $50M$ (where M is the total mass) [10]. An open issue is therefore to find methods that allow longer lasting evolutions of two black holes before they merge, ideally allowing evolution times on the order of 1 or more orbital periods.

In this Letter we present results for a new method to choose comoving coordinates that makes it possible to evolve two black holes for about one orbital period for the first time. The black holes start out close to but well outside the ISCO, and the apparent horizons (AHs) do not merge before one orbital period has passed. Since there are many different choices for the various components of a numerical relativity simulation that crucially affect its quality, we first describe each one of them in sufficient detail to establish our basic framework. We then discuss the major new aspect of our method, how we construct comoving coordinates, and discuss our numerical results.

As initial data we choose puncture data [11] for two equal mass black holes without spin on a quasicircular orbit based on an approximate helical Killing vector [12,13]. Each configuration is determined by the coordinate distance ρ_0 of the punctures from the origin. We focus on $\rho_0 = 3.0M$, where M is the total ADM (Arnowitt-Deser-Misner) mass at the punctures. For $\rho_0 = 3.0M$, the ADM mass at infinity is $0.985M$, the bare mass of one puncture is $0.477M$, the size of the linear momentum of the individual black holes is $0.138M$, the angular velocity is $0.0550/M$, and the orbital period is $T = 114M$. For comparison, post-Newtonian methods and the thin-sandwich approach find the ISCO in the neighborhood of $T = 65M$ [14], which translates to about $\rho_0 = 1.9M$ in our method. The effective potential method locates the ISCO near $\rho_0 = 1.1M$ and $T = 35M$ [15,16].

As an evolution system we use the modified version of the Baumgarte-Shapiro-Shibata-Nakamura (BSSN) system that is described in detail in [17]. At the outer boundary we impose a radiative boundary condition [17] (we did not implement the monopole term). The black holes are handled by introducing a time independent excision boundary according to the "simple excision" method described in [18], with a generalization from cubical to spherical excision regions. We also perform control runs without excision using the puncture evolution method [4,17], which typically do not last as long as the excision runs, but which allow us to check the excision method.

As coordinate conditions we use the dynamic gauge conditions that proved to be successful for single black hole runs with and without excision [17–19] and for head-on collisions [17]. For the lapse we choose "1 + log" slicing without explicit shift dependence, and for the shift we use a particular version of the "Gamma driver" condition:

$$\partial_t \alpha = -2\alpha K \psi^m, \tag{1}$$

 © 2004 The American Physical Society

$$\partial_t \beta^i = \tfrac{3}{4}\alpha^p \psi^{-n} B^i, \qquad \partial_t B^i = \partial_t \tilde{\Gamma}^i - \eta B^i, \qquad (2)$$

where α is the lapse, β^i is the shift, B^i is its first derivative, K is the trace of the extrinsic curvature, $\tilde{\Gamma}^i$ is the contracted conformal Christoffel symbol of BSSN, and ψ is the time independent conformal factor of Brill-Lindquist data. After some experimentation we settled for our binary runs on $m = 4$, which helps mimic the singularity avoidance of maximal slicing for puncture runs, and for the shift we set $n = 2$, $p = 1$, and $\eta = 2/M$.

One important point to be made about the gauge conditions (1) and (2) is that although they work well for black holes without linear momentum, they do not impose corotating or comoving coordinates. Moving the black hole excision region is showing a lot of promise [20], but here we attempt to minimize the dynamics around black holes at fixed coordinate positions by modifying the shift condition. Corotating frames for numerical relativity are used, for example, in [21] and with dynamic adjustments in [10,22]. The method that we have developed as a first step toward long term comoving coordinates is an extension of the methods and ideas of [10,22] to orbiting configurations.

In order to obtain approximately comoving coordinates we introduce the shift vector

$$\beta^i_{com} = \psi^{-q}[A_1 \omega(-y, x, 0)^i + A_2 \dot{r}(-x, -y, 0)^i], \qquad (3)$$

where x, y, and z denote Cartesian coordinates, with $\rho = (x^2 + y^2)^{1/2}$ and $r = (\rho^2 + z^2)^{1/2}$. The first term inside the brackets is a rotation about the z axis with angular velocity $A_1\omega$, while the second term is an inward radial motion with radial velocity $A_2\dot{r}\rho$. The factor ψ^{-q} is used to attenuate the shift to zero at each puncture, which is needed for simulations without excision. Clearly, for two point particles on an inspiraling orbit this shift can cancel the dynamics of the point particles completely. For two orbiting black holes we can compensate only some aspects of the global motion, similar to balancing the bulk motion of two stars, with some dynamics remaining in the metric.

For the runs reported below we have set $q = 3$, because this results in the natural falloff of the shift near punctures [17], and we use the same value with excision. The prefactor A_1 can be used to attenuate the angular shift for large r [10], which simplifies the outer boundary and the analysis at large r at the cost of introducing additional differential rotation, but for now we work with $A_1 = 1$. Since ψ^{-3} tends to 1 for $r \to \infty$, the shift corresponds to a rigid rotation for large r, in particular, the coordinate motion becomes superluminal beyond a light cylinder. For the radial shift we attenuate with $A_2 = (c^2 + 1)^s/[\rho_0(c^2 + \rho^2/\rho_0^2)^s]$, which is constructed such that at the initial radial distance ρ_0 to the black holes the norm of $A_2(x, y, 0)^i$ is unity, at the origin the norm is zero, for large ρ the falloff is controlled by s, and the shape of the attenuation can be adjusted with c. We set $c = 1$ and $s = 2$.

To evolve for one orbital time scale it was necessary to introduce a dynamic control mechanism with time dependent velocities $\omega(t)$ and $\dot{r}(t)$ in the commotion shift (3) (see also [22]). In order to estimate changes in these velocities we define the vector $a^i(t) = \sum(x^i_{\text{puncture}} - x^i)\alpha(t)/\sum \alpha(t)$, where the sums run over all points on the excision boundary in the orbital plane. The vector $a^i(t)$ points from the center of the excision region (from the puncture) in the direction into which the lapse profile has moved off center. At finite time intervals Δt, we use $a^i(t)$ to compute a velocity correction

$$\Delta v^i = [-\gamma_{\text{damp}} \partial_t a^i(t) - k_{\text{drive}} a^i(t)]\Delta t, \qquad (4)$$

which is designed to damp out motion in $a^i(t)$ and to drive $a^i(t)$ back to zero as in a damped harmonic oscillator. In coordinates where the punctures are located on the y axis, Δv^i defines changes in $\omega(t)$ and $\dot{r}(t)$ by $\Delta\omega = \Delta v^x/\rho_0$ and $\Delta\dot{r} = \Delta v^y$. In our case, useful values for the coefficients are $k_{\text{drive}} = 0.2/M$ and $\gamma_{\text{damp}} = 5$.

The evolution of the shift proceeds as follows. We set the initial lapse to one and initialize the shift according to (3), for example, with $\omega = 0.88\Omega$ and $\dot{r} = 0$ for $\rho_0 = 3M$, where Ω is the angular velocity at infinity defined by the initial data. Note that close to the black holes a correction to Ω is necessary but not unexpected. At each time step during the evolution, we evolve the shift with (2). First, we evolve for a time interval of $5M$ without any commotion correction until lapse and shift have gone through their first rapid evolution to adjust themselves to the presence of the black holes. After that we compute $\Delta\omega$ and $\Delta\dot{r}$ based on (4) at resolution independent time intervals of $\Delta t = 2M$, which defines a shift vector $\Delta\beta^i$ according to (3). This shift vector $\Delta\beta^i$ is added to β^i everywhere on the grid, so the shift changes discontinuously at intervals of Δt, but we leave the time derivative B^i unchanged.

Assuming a rigidly rotating frame at large distances, we generalize the radiative boundary condition taking into account that the scalar wave propagation no longer happens along the radial direction, and that tensor components have to be rotated to the new frame. For any tensor F (indices suppressed) the result is

$$\partial_t F = \mathcal{L}_\beta F - v\frac{x^k}{r}(F - F_\infty)_{,k} - v\frac{F - F_\infty}{r}, \qquad (5)$$

where $\mathcal{L}$ is the Lie derivative, v is the wave speed, and F_∞ is the value of F at infinity. We have experimented with cubical and spherical outer boundaries, where the latter is expected to have less problems with a global rotation. A superluminal shift does not create a problem in our runs with the outer boundary at $24M$, $48M$, or $96M$, since we can lower the Courant factor in the outer regions of our fixed mesh refinement grid, which we describe below, by switching from Berger-Oliger time stepping to uniform time steps.

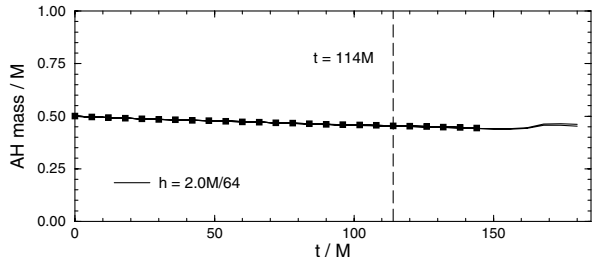

FIG. 1. Evolution of the AH mass for the black hole binary with $\rho_0 = 3.0M$. The evolution lasts longer than one orbital period of $114M$ defined by the initial data. The squares mark a run with seven nested levels with coarsest resolution $2M$ and finest resolution $h = 0.031\,25M$, and with the spherical outer boundary at about $48M$, which crashes around $145M$. Also plotted are results from seven control runs with the outer boundary at $24M$ and $96M$, with a cubical outer boundary, and with the AH extracted on a coarser grid to check its convergence. There is little difference in the results, except that the runs with the boundary at $24M$ last somewhat longer.

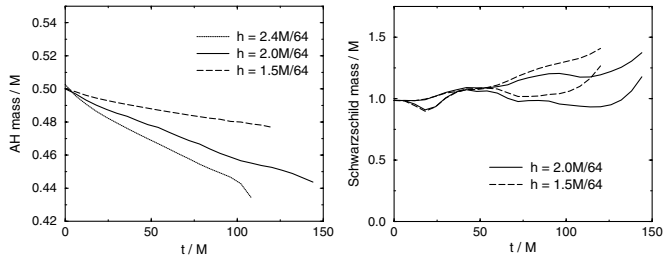

FIG. 2. The panel on the left shows convergence of the AH mass. The number and size of the refinement levels was not changed, but the overall resolution was rescaled by a constant factor. There is a linear downward drift in the mass which becomes smaller with increasing resolution. The panel on the right displays the mass at infinity estimated on a sphere of radius $20M$ assuming a Schwarzschild background, showing fluctuations of about 20% to 40%. The lower and upper lines for a given resolution correspond to a cubical outer boundary at $24M$ and $48M$, respectively.

All evolutions are carried out with a new version of the BAM ("bi-functional adaptive mesh") code [23], which is built around an oct-tree, cell-centered adaptive mesh kernel that currently is functional for fixed mesh refinements (FMR) without parallelization. Adaptive mesh refinement (AMR) was made famous in numerical relativity by Choptuik's work on critical collapse [24], and especially in 3D it can offer enormous savings over conventional unigrid codes. However, while the basic technical problem of writing AMR codes has been solved many times, see, e.g. [25] for an overview and [26–29] for some recent applications in numerical relativity, there have been only a handful of examples for the full 3D Einstein equations and the evolution of one [30–32] or two [4] black holes. The FMR technique with the nested boxes of [30] was essential for the feasibility of the first 3D grazing collision [4].

One aspect of the present Letter is that we demonstrate that FMR can work successfully even for black holes in an orbital configuration. We use nested Cartesian boxes, where for black hole binaries with equal mass and no spin we have to store only one quadrant of the global domain. BAM's Berger-Oliger FMR algorithm uses third order polynomial interpolation in space and second order polynomial interpolation in time, following essentially the recipe of [4,30]. The main missing feature was a reasonably stable unigrid code, which is now available in the form of BSSN with dynamic gauge as discussed above. An important detail of our setup is the use of the iterative Crank-Nicolson method for time integration. To avoid special boundary conditions during Crank-Nicolson iterations, BAM uses three buffer points [32].

Let us summarize our numerical results. For the black hole binary with $\rho_0 = 3.0M$ introduced above, evolution times of up to $185M$ are obtained and a typical run easily exceeds the orbital period of $114M$. Figure 1 shows the AH mass for one of the black holes as a function of time.

It is important to note that a common AH enclosing both black holes does not form within the achieved evolution time, while for sufficiently small values of ρ_0 (and the same AH finder described in [33] and implemented in CACTUS [34]) a common AH is found in [10].

There is an almost linear drift in the AH mass of about 10% per $100M$ at a resolution of $h = M/32$ near the excision region, which becomes smaller with increasing resolution as shown in Fig. 2. (We have also evolved Schwarzschild on quadrants and full grids for $1000M$ and more, confirming that our FMR method is convergent in the AH mass.) Puncture evolutions without excision give a quantitatively very similar result; hence the simple excision technique does not appear responsible for the drift. Since the AH is a slice dependent quantity, the warpage of the slice contributes to changes in the AH mass. The proper spatial distance between the AHs along the y axis starts at about $9M$, rises to $11M$, and drops to $7M$ at $t = 140M$, but since this distance depends on the gauge and since it does not converge for the current resolutions, this is only a preliminary result. In the future we plan to find event horizons to resolve some of the ambiguity. Figure 2 also shows an estimate for the mass

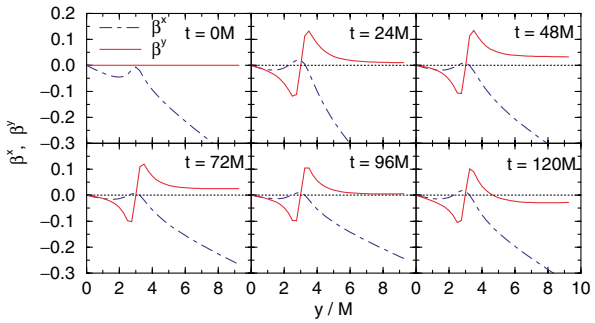

FIG. 3 (color online). Evolution of the x and y components of the shift vector along the y axis. The punctures are located on the y axis at $y = \pm 3M$.

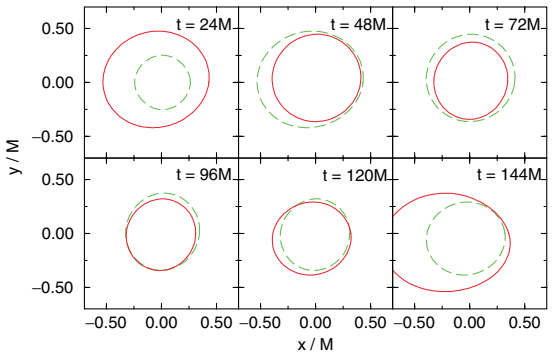

FIG. 4 (color online). Evolution of the AH of one of the black holes in the x-y plane. The dashed line shows the AH at $t - 24M$ in each panel. Initially, the AH moves outward quickly while the gauge adjusts itself near the black hole. It then slowly shrinks toward the center while being deformed slightly until eventually it drifts out of shape before the run fails around $145M$. Note that the proper area changes linearly and only on the order of 10% during the entire run; see Fig. 1.

at infinity. The errors are satisfactory for the present purpose. Since the AH mass shown in Fig. 1 is not significantly affected by the location of the outer boundary, we conclude that the interior of the numerical domain has been computed with good accuracy.

Figure 3 shows the evolution of the shift vector. In particular, the corotation speed initially increases, then decreases slowly before increasing again towards the end. As an indication of the remaining coordinate motion near the black holes we show the evolution of the AH in Fig. 4. A residual drift of similar magnitude is observed also for larger separations, which is a likely reason for the code failure that occurs after about $150M$ rather independently of separation up to $\rho_0 = 12M$.

In conclusion, dynamically adjusted comoving coordinates enable us to perform the first numerical simulations of two black holes near but outside the ISCO for about one orbital period. A good indicator for one orbit would be the presence of two cycles of gravitational waves. First experiments with wave extraction indicate that improvements of the outer boundary are needed.

It is a pleasure to thank M. Alcubierre, P. Diener, N. Dorband, S. Hawley, D. Pollney, E. Seidel, and the AEI team for many discussions and collaborations on the methods on which our simulations are based. S. Hawley performed the first experiments with a dynamic corotation shift in the context of [10]. We also thank A. Ashtekar and P. Laguna for discussions, and we thank B. Lacki for help with HDF5. We acknowledge the support of the Center for Gravitational Wave Physics funded by the National Science Foundation under Cooperative Agreement No. PHY-01-14375. This work was also supported by NSF Grants No. PHY-02-18750 and No. PHY-02-44788.

[1] K. Thorne, Rev. Mod. Phys. **52**, 285 (1980).
[2] B. Schutz, Classical Quantum Gravity **16**, A131 (1999).
[3] P. Anninos, K. Camarda, J. Massó, E. Seidel, W.-M. Suen, and J. Towns, Phys. Rev. D **52**, 2059 (1995).
[4] B. Brügmann, Int. J. Mod. Phys. D **8**, 85 (1999).
[5] S. Brandt *et al.*, Phys. Rev. Lett. **85**, 5496 (2000).
[6] M. Alcubierre, W. Benger, B. Brügmann, G. Lanfermann, L. Nerger, E. Seidel, and R. Takahashi, Phys. Rev. Lett. **87**, 271103 (2001).
[7] J. Baker, B. Brügmann, M. Campanelli, C. O. Lousto, and R. Takahashi, Phys. Rev. Lett. **87**, 121103 (2001).
[8] J. Baker, B. Brügmann, M. Campanelli, and C. O. Lousto, Classical Quantum Gravity **17**, L149 (2000).
[9] J. Baker, M. Campanelli, C. O. Lousto, and R. Takahashi, Phys. Rev. D **65**, 124012 (2002).
[10] M. Alcubierre *et al.* (to be published).
[11] S. Brandt and B. Brügmann, Phys. Rev. Lett. **78**, 3606 (1997).
[12] W. Tichy, B. Brügmann, and P. Laguna, Phys. Rev. D **68**, 064008 (2003).
[13] W. Tichy and B. Brügmann, Phys. Rev. D **69**, 024006 (2004).
[14] T. Damour, E. Gourgoulhon, and P. Grandclement, Phys. Rev. D **66**, 024007 (2002).
[15] G. B. Cook, Phys. Rev. D **50**, 5025 (1994).
[16] T. W. Baumgarte, Phys. Rev. D **62**, 024018 (2000).
[17] M. Alcubierre, B. Brügmann, P. Diener, M. Koppitz, D. Pollney, E. Seidel, and R. Takahashi, Phys. Rev. D **67**, 084023 (2003).
[18] M. Alcubierre and B. Brügmann, Phys. Rev. D **63**, 104006 (2001).
[19] M. Alcubierre, B. Brügmann, D. Pollney, E. Seidel, and R. Takahashi, Phys. Rev. D **64**, 061501(R) (2001).
[20] U. Sperhake, K. L. Smith, B. Kelly, P. Laguna, and D. Shoemaker, Phys. Rev. D **69**, 024012 (2004).
[21] M. D. Duez, P. Marronetti, S. L. Shapiro, and T. W. Baumgarte, Phys. Rev. D **67**, 024004 (2003).
[22] M. Alcubierre, P. Diener, F. S. Guzmán, S. Hawley, M. Koppitz, D. Pollney, and E. Seidel (to be published).
[23] B. Brügmann (to be published).
[24] M. W. Choptuik, Phys. Rev. Lett. **70**, 9 (1993).
[25] T. Plewa, http://flash.uchicago.edu/~tomek/amr.
[26] P. Diener, N. Jansen, A. Khokhlov, and I. Novikov, Classical Quantum Gravity **17**, 435 (2000).
[27] D.-I. Choi, J. D. Brown, B. Imbiriba, J. Centrella, and P. MacNeice, J. Comput. Phys. **193**, 398 (2004).
[28] M. W. Choptuik, E. W. Hirschmann, S. L. Liebling, and F. Pretorius, Phys. Rev. D **68**, 044007 (2003).
[29] F. Pretorius and L. Lehner, gr-qc/0302003.
[30] B. Brügmann, Phys. Rev. D **54**, 7361 (1996).
[31] G. Lanfermann, Master's thesis, MPI für Gravitationsphysik, Freie Universität Berlin, 1999.
[32] E. Schnetter, S. H. Hawley, and I. Hawke, Classical Quantum Gravity **21**, 1465 (2004).
[33] M. Alcubierre, S. Brandt, B. Brügmann, C. Gundlach, J. Massó, E. Seidel, and P. Walker, Classical Quantum Gravity **17**, 2159 (2000).
[34] CACTUS, http://www.cactuscode.org.